

Real-time LPI-based Assessment of the Liquefaction Potential of the Incheon Port in Korea

H.S. Kim, N.G. Cho & C.K. Chung

Department of Civil and Environmental Engineering, Seoul National University, Seoul, Korea



SUMMARY:

Recent cases of liquefaction hazards in harbor areas invoke the necessity of seismic study in Korea, as liquefaction is a significant threat to structures in harbor areas. Therefore in this study, a real-time assessment of the liquefaction potential was performed at Incheon port, which is 40 km from downtown Seoul. A simplified systematic framework with a computer-based spatial information system was utilized. According to the framework, the factor of safety for the liquefaction of each soil layer (Cyclic Stress Ratio/Cyclic Resistance Ratio) was estimated. The liquefaction potential at the target point was then evaluated by the liquefaction potential index (LPI) proposed by Iwasaki et al. (1978). The LPI was computed by integrating the FS values over the depth of liquefaction-susceptible soil layers, providing an estimate of liquefaction-related surface damage. For applicable examples, two earthquake events were utilized. The results were visualized on a location map to confirm the applicability of the proposed framework for the real-time assessment of the liquefaction potential.

Keywords: liquefaction probability, port, LPI, real-time, GIS

1. INTRODUCTION

Historically, the Korean peninsula has been regarded as a safe region with respect to the hazard of liquefaction due to the characteristics of its location, being classified as a region of moderate seismicity. However, recent cases of liquefaction hazards in harbor areas invoke the necessity of seismic study in Korea, as liquefaction is a significant threat to structures in harbor areas, such as quay walls and gantry cranes on seismically vulnerable reclaimed soil deposits. Therefore, evaluation of the liquefaction potential for harbor areas has been recently emphasized in Korea.

Liquefaction can be triggered by the rapid loading invoked by seismic shear-wave energy when there is insufficient time for excess pore-water pressure to dissipate through natural drainage. It can also be triggered by rapid straining along discrete horizons, such as landslides and lateral spreads. Any type of rapid loading situation that serves to elevate the pore-water pressure can result in cyclic softening in fine-grained materials or liquefaction in porous materials of low relative density with little or no cohesion (Idriss and Boulanger 2008).

Different types of liquefaction damage, such as landslides, lateral spreads and sand boil events, have occurred at harbor sites because harbors are constructed in limited area near coasts and earthworks such as dredge and reclamation are executed frequently. When widespread liquefaction occurred in Kobe, Japan, during the 1995 Hyogoken-Nanbu earthquake, large-scale liquefaction was documented by acceleration records from a downhole seismic array. The reclaimed Port Island in Kobe suffered major liquefaction-induced damage as well as indirect damage, such as sliding and overturning of the quay wall and a collapse of harbor structures.

Even if an earthquake occurred unexpectedly and suddenly, rapid estimation of earthquake damage potentials over the target area is essential to minimize damage and to provide an effective means of emergency control. In this study, a real-time assessment of the liquefaction potential was conducted at the Incheon port based on a computer-based spatial information system. This framework functions as a database for site investigations and for the automatic transmission of seismic monitoring data. For the real-time approach, the values of the cyclic resistance ratio (CRR) for the liquefaction resistance were

estimated in advance at various locations around the site with available borehole SPT data. The values of cyclic stress ratio (CSR) causing liquefaction were computed with seismic loads via the transmitted seismic monitoring information, where the seismic loads were computed by predetermined correlations of the ground motions of each soil layer at the site above the base rock. The factor of safety for the liquefaction of each soil layer (CSR/CRR) was estimated. Finally, the liquefaction potential was evaluated by the liquefaction potential index (LPI) proposed by Iwasaki et al. (1978). The LPI was computed by integrating the FS values over the depths of the liquefaction-susceptible soil layers, providing an estimate of the liquefaction-related surface damage. For applicable examples, two earthquake events (the Odaesan Earthquake in 2007 and the Great East Japan Earthquake in 2011) were utilized. The results were visualized on a location map of the site to confirm the applicability of the proposed framework for the real-time assessment of the liquefaction potential.

2. ASSESSMENT OF LIQUEFACTION POTENTIAL

2.1. Liquefaction Potential Evaluation

Assessing the liquefaction potential is an important issue in geotechnical earthquake engineering. Several methods have been proposed to evaluate the liquefaction potential of sandy soils. In-situ tests such as the standard penetration test (SPT), the cone penetration test (CPT), the Becker penetration test (BPT) and field measurements of the shear wave velocity (V_s) are used as empirical tools to evaluate the CRR of a soil layer which may liquefy during an earthquake (Youd et al. 2001). An empirical criterion based on SPT-N values is commonly used in liquefaction assessments in most countries, including Korea. Seed and Idriss (1971) proposed a simplified procedure based on SPT-N values for the evaluation of the liquefaction resistance of soils after two large and catastrophic earthquakes occurred in Alaska and in Niigata (Japan) in 1964. The original simplified procedure based on empirical rules has been modified and improved over the years (Seed 1983, Seed et al. 1985, Seed and DeAlba 1986, Seed and Handler 1990). Later, Youd et al. (2001) proposed the following form:

$$CRR_{7.5} = \frac{1}{34 - (N_1)_{60}} + \frac{(N_1)_{60}}{135} + \frac{50}{[10(N_1)_{60} + 45]^2} - \frac{1}{200} \quad (2.1)$$

Here, $CRR_{7.5}$ is the cyclic resistance ratio for an earthquake magnitude (M) of 7.5 and $(N_1)_{60}$ is the value of the field-measured N value corrected for hammer efficiency and the effective overburden stress.

$CRR_{7.5}$ is calibrated using the magnitude scaling factor (MSF) according to the current seismic design code in Korea with an earthquake magnitude (M) of 6.5:

$$CRR_{6.5} = CRR_{7.5} \times MSF \quad (2.2)$$

Here, $MSF = 10^{2.24/M^{2.56}} = 1.44$.

The factor of safety (FS) against the liquefaction of a saturated soil is expressed as the ratio of the cyclic resistance ratio (CRR) to the cyclic stress ratio (CSR). The CSR is expressed as

$$CSR = 0.65 \left(\frac{a_{\max}}{g} \right) \left(\frac{\sigma_v}{\sigma_v'} \right) (\gamma_d) / MSF \quad (2.3)$$

where σ_v is the total vertical stress at depth (z); σ_v' denotes the effective vertical stress; a_{\max} is the peak acceleration of each layer; g represents the acceleration of gravity; and γ_d is the stress reduction factor. In this study, the term γ_d is estimated using the equation formulated by Liao and

Whitman (1986):

$$\gamma_d = 1.0 - 0.00765 \times z \quad \text{for } z \leq 9.15\text{m} \quad (2.4a)$$

$$\gamma_d = 1.174 - 0.0267 \times z \quad \text{for } 9.15\text{m} \leq z \leq 23\text{m} \quad (2.4b)$$

The factor of safety against liquefaction per layer, FS, is calculated as the ratio of $CRR_{6.5}$ (cyclic resistance ratio) to the CSR (cyclic stress ratio) based on a deterministic procedure widely known as the “simplified procedure” (Seed and Idriss 1971, Seed et al. 1985, Youd et al. 2001).

$$FS_{\text{liquefaction}} = \frac{CRR_{6.5}}{CSR} \quad (2.5)$$

The conditions of $FS > 1$ and $FS < 1$ indicate that the soils are classified as non-liquefiable and liquefiable, respectively, while the $FS = 1.0$ represents the limiting equilibrium.

The FS value as determined from the conventional procedure is not a sufficient tool by itself for the evaluation of the liquefaction potential. The severity of foundation damage caused by soil liquefaction cannot be accessed directly by the FS, specifically in cases that depends on the severity of liquefaction. The damage caused by liquefaction under the following conditions tends to be severe (Iwasaki and others 1982):

1. The liquefied layer is thick.
2. The liquefied layer is shallow.
3. The FS value of the liquefied layer is far less than 1.0.

2.2. Liquefaction Potential Index (LPI)

In order to evaluate the liquefaction potential of ground surface, Iwasaki et al. (1978, 1982) proposed the use of an index which is proportional to the thickness of the liquefiable layer and the value of the factor of safety against liquefaction of each layer. A weighting function gives higher values to the layers closest to the ground surface, and decreases linearly to zero, at a depth of 20 m. The Liquefaction Potential Index (LPI) defined by Iwasaki et al. (1978, 1982) can be expressed as follows:

$$LPI = \int_0^{20} F(z)W(z)dz \quad (2.6)$$

$$F(z) = 1 - FS \quad \text{for } FS < 1.0 \quad (2.7a)$$

$$F(z) = 0 \quad \text{for } FS \geq 1.0 \quad (2.7b)$$

$$W(z) = 10 - 0.5z \quad \text{for } z \leq 20\text{m} \quad (2.8a)$$

$$W(z) = 0 \quad \text{for } z > 20\text{m} \quad (2.8b)$$

Here, z denotes the depth ($0 \sim 20\text{m}$); dz denotes the increment of depth; and $F(z)$ represents the liquefaction severity, which is a function of the FS defined in Eqn. 2.7a and b. Finally, $W(z)$ is the weighting function as defined in Eqn. 2.8a and b.

This study used a discretized form (Luna 1995, Luna and Frost 1998) to find the LPI, given as

$$LPI = \sum_{i=1}^n F_i(z)W_i(z)H_i \quad (2.9)$$

where n denotes the number of discretized layers, H_i is the thickness of the discretized layer, and F_i denotes the liquefaction severity for layer i .

Iwasaki et al. (1982) calibrated the values of LPI with the severity of liquefaction induced damage using data mostly for sandy soils, as provided by 87 SPT borings in liquefied and non-liquefied sites in

Japan. This method was adopted to evaluate the liquefaction potential in North America (Luna 1995, Luna and Frost 1998, Toprak and Holzer 2003, Holzer et al. 2006).

Iwasaki et al. (1978, 1982) found that severe liquefaction and minor liquefaction are likely to occur whenever the LPI is greater than 15 and the LPI is less than 5, respectively. The LPI value is inversely proportional to the FS and the depth of the saturated layers; the higher the index, the greater the potential for liquefaction. The categories of liquefaction severity were modified by Luna and Frost (1998) and Chung et al. (2011) and are summarized in Table 2.1. Also, the category adopted in this study is proposed, as discussed below.

Table 2.1. Historic liquefaction severity assessed from the liquefaction potential index (LPI)

LPI	<i>Iwasaki et al.(1982)</i>	<i>Luna and Frost(1998)</i>	<i>Chung et al.(2011)</i>	<i>This study</i>
0	Not likely	Little to none	None	Very low
$0 < \text{LPI} \leq 5$	Minor	Minor	Little to none	Low
$5 < \text{LPI} \leq 15$	-	Moderate	Moderate	High
$15 < \text{LPI} \leq 100$	Severe	Major	Severe	Very high

2.3. Real-time LPI-based Assessment of Liquefaction Potential

The real-time LPI-based systematic assessment of liquefaction potential for harbor site is suggested in Fig. 2.1. A simplified systematic framework with a computer-based spatial information system was adopted to provide the estimation of the real-time liquefaction hazard. This framework also functions as a database system for site investigations and for the automatic transmission of seismic monitoring data at the harbor sites.

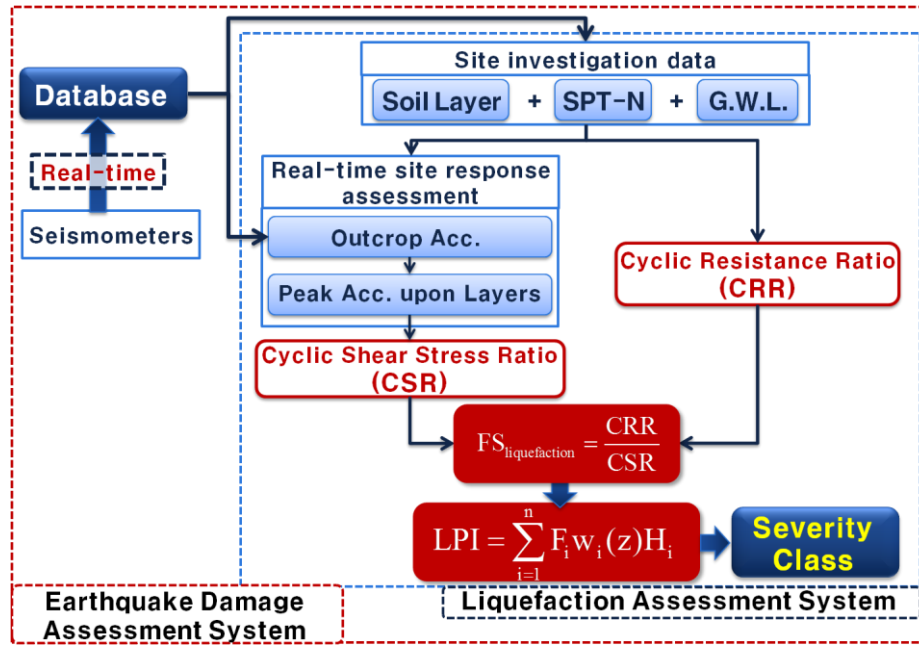


Figure 2.1. Real-time LPI-based assessment of liquefaction potential

The collected site investigation datasets were installed in the database in advance. In addition, the seismic monitoring datasets as recorded from a seismometer were transmitted and stored in the database in real time. When an earthquake occurred at a target harbor site, the seismic events were recorded by the seismic monitoring system and they were also transmitted and stored in this system. Initially in this assessment, the ground conditions of the target area for the liquefaction estimations are analyzed from the system database. The basic conditions for the liquefaction assessment are as follows: (1) within a depth of 20m; (2) below the ground water level (G.W.L.); (3) under 20 (the SPT-N value); and (4) a condition consisting of fill, alluvial and weathered residual soils. In the current standard, the depth of liquefaction can be influenced by the ground being less than 20m;

though if necessary, a depth of more than 20m can be reviewed. To estimate the G.W.L. condition, the highest G.W.L. considering fluctuations such as the effects of tides and rainfall should be selected. A daily average highest G.W.L. during the monitoring period from the annual G.W.L. record at the target port was applied here.

Second, the cyclic stress ratio (CSR) values causing liquefaction are computed with the seismic loads from the transmitted seismic monitoring information, where the seismic loads are computed by predetermined correlations between the ground motions of the bedrock and the overlying individual soil layers. Site response analyses at borehole locations with Pro-Shake were performed in advance with inputs of varying accelerations of outcrop rock and three seismic waveforms of the Hachinohe, Ofunato and artificial earthquake records (Table 2.2), and correlation equations between the outcrop and peak acceleration values for each soil layer were predetermined based on nonlinear optimization of a regression model according to the flow chart shown in Fig. 2.2.

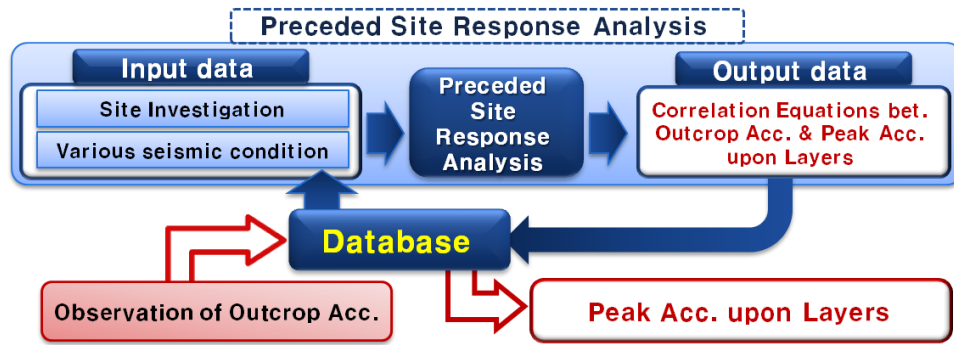
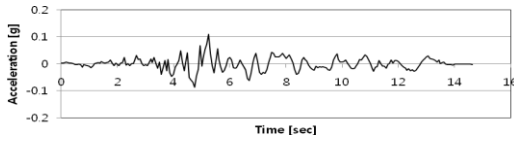
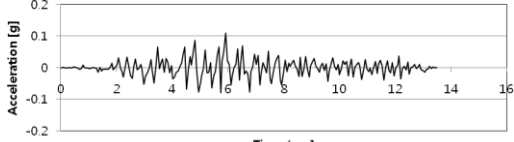
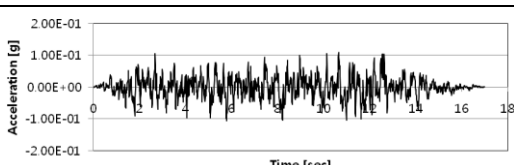


Figure 2.2. Real-time site response assessment

Table 2.2. The magnitude and time history of the seismic records

Earthquake	Magnitude	Date	Location	Site Condition	Time History
Hachinohe	7.9	05/16/68	Tokachioki, Japan	S _C	
Ofunato	7.4	12/06/78	Miyagikenoki, Japan	S _D	
Artificial	-	-	-	S _B	

The established correlation equation between the outcrop acceleration and peak acceleration of each layer is expressed as follows:

$$a_{\max} = \alpha \left(1 - e^{-\beta \cdot a_{\text{outcrop}}} \right) \quad (2.11)$$

Here a_{\max} denotes peak acceleration of each layer; a_{outcrop} represents the measured outcrop acceleration, and α and β are correlation coefficients. The CSR is determined by Eqn. 2.3 with the computed a_{\max} value for the corresponding layer by the above equation, where the a_{outcrop} value is

transmitted from data recorded by the seismometer at the target harbor site in real time.

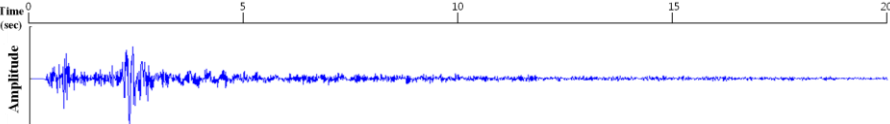
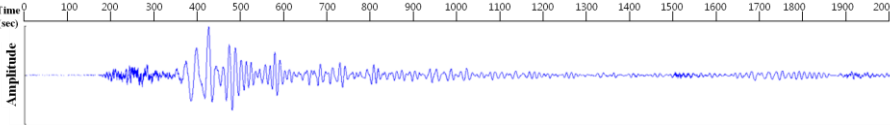
Third, the CRR value was computed using Eqn. 2.1 and 2.2 based on the ground conditions of the target area. Fourth, the FS value for the liquefaction potential of each liquefiable soil layer was estimated by Eqn. 2.5. Finally, the LPIs were determined by Eqn. 2.9 for individual borehole locations.

3. SIMULATION OF THE LIQUEFACTION ASSESSMENT OF INCHEON PORT IN KOREA

3.1. Simulation Condition

For the application examples, two earthquake events (the Odaesan Earthquake in 2007 and the 2011 Great East Japan Earthquake) were utilized to verify the proposed assessment. For the Odaesan Earthquake (Magnitude 4.8), seismic data monitored at the nearest location (13km) was utilized. For Great East Japan Earthquake (Magnitude 9.0), monitored record at 130km off from epicenter was applied. The seismic waves of two earthquake events are shown in Table 3.1.

Table 3.1. The magnitude and seismic waves of the two earthquake events

Earthquake	Magnitude	Seismic Waves
Odaesan Earthquake -scale	4.8	
Great East Japan Earthquake -scale	9.0	

At the Incheon port, the target areas were divided into three sites (A, B and C) and a total of 22 site investigation borehole data points were used (Fig. 3.1). From the design report and satellite images of the target area, sites A and B consists of a gravity quay wall and general building structures. Site C is a container terminal, including a landing pier and a gantry crane. Ground coverage at the Incheon port has varied over the last 40 years due to dredging and soil reclamation events. Thus, the soil conditions have changed over time. The ground coverage conditions for each borehole location based on aerial photographs in 1975, 1980 and 2012 are given as water, wet land and built-up land by reclamation efforts.

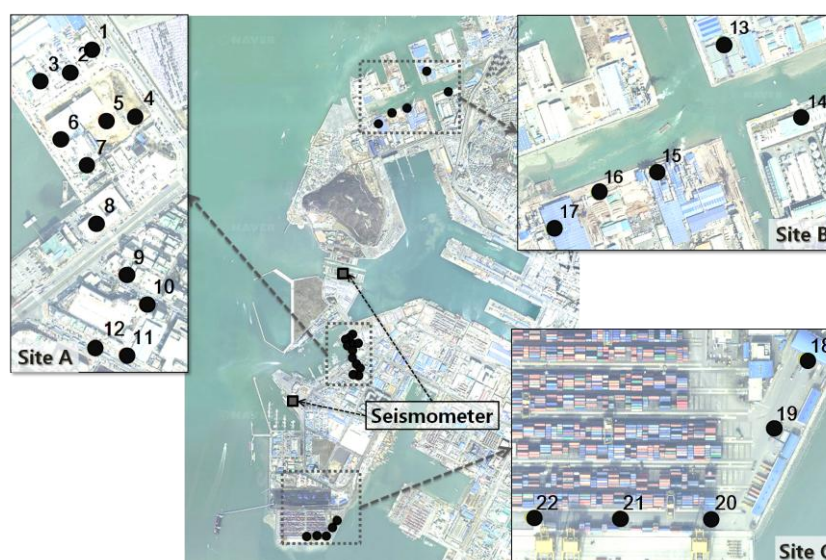


Figure 3.1. Target areas (site A, B & C) of the Incheon port

Table 3.2 shows the site conditions for the target areas based on the borehole data. The G.W.L. was determined from the daily average record monitored at a well installed at the Incheon port. Fill soil partly covered site A, and mostly covered sites B and C. This soil consisted of mixed materials with reclaimed soil deposits from offshore areas and boulder stone quarried from a nearby mountain. Alluvial soils consisted of silty sand or silty clay, which underlie the fill. The underlying weathered residual soil above the weathered rock can be classified as hard sandy materials. Given this site condition, the sandy stratum was characterized as material susceptible to liquefaction, while the clayey material is considered to be non-liquefiable. The ground conditions for liquefaction potential estimation do not rely on the soil layer itself but on the condition of liquefiable soils such as the G.W.L., the material properties and the SPT-N value.

Table 3.2. Site condition of the target areas of the Incheon port

Site	Boring Year	No.	Elev.	G.W.L.(-m)	Soil Thickness(m)				Ground Coverage Condition(year)		
					F	AS	WS	WR	1975	1980	2012
A	2002	1	8	3	-	6	-	5	waters	built-up	built-up
		2	8	4.9	-	5.8	-	5.2	waters	built-up	
		3	8	4.8	-	7	-	5	waters	wet land	
		4	8	0.1	8	8	-	5	waters	built-up	
		5	8	5.0	-	8.8	-	5.2	waters	built-up	
		6	8	5.4	-	7	-	5	waters	built-up	
		7	8	0.1	10.2	8.4	-	1	waters	wet land	
		8	8	3.0	-	9	-	5	built-up	built-up	
		9	8	2.8	-	11.5	-	5	built-up	built-up	
		10	8	0.7	-	12.9	-	5.1	built-up	built-up	
		11	8	0.5	8.3	21.2	-	5	wet land	built-up	
		12	8	1.5	-	19	-	5	wet land	built-up	
B	2001	13	7.5	6.8	5.9	18.6	1.9	5.6	waters	wet land	built-up
		14	7.5	6.3	7	14.9	3.4	6.2	wet land	wet land	
		15	7.5	6.7	6	18.2	-	2.7	bare land	wet land	
		16	7.5	7.0	7.5	21.7	-	0	bare land	wet land	
		17	7.5	7.0	6.5	10	-	4.5	bare land	built-up	
C	2011	18	7.2	3.0	6.5	10	4	1	waters	wet land	built-up
		19	7.2	4.9	7.3	5.7	4.8	1	waters	wet land	
		20	7.2	4.8	6.2	4.3	6.5	2.5	waters	wet land	
		21	7.2	0.1	6.5	2.5	5	3	waters	wet land	
		22	7.2	5.0	7.3	4.8	1	-	waters	waters	

Note: F = Fill Soil; AS = Alluvial Soil; WS = Weathered Residual Soil; WR = Weathered Rock.

3.2. Simulation Results

Based on the site investigation data in Table 3.2, a liquefaction assessment was conducted for the target area for the two earthquake events. The simulation results are shown in Table 3.3. The liquefiable layer was determined based on the liquefiable soil condition from the original soil layer. The peak ground accelerations for each layer were also determined by the applied earthquake events based on the real-time site response assessment.

The quantitative FS value pertaining to the liquefaction potential of each liquefiable soil layer was analyzed. According to the LPI values, the liquefaction severity results in Table 2.1 were determined for every data point.

For the Odaesan Earthquake event, two locations at site A were determined as having ‘High’ liquefaction potential, while the others showed ‘Very low’ or ‘Low’ potential. For the 2011 Great East Japan Earthquake event, all of site A was as ‘Very high’ or ‘High’. Meanwhile, sites B and C were regarded as safe regions for liquefaction, classified as having ‘Very low’ potential, except for the No. 21 borehole location. It is because at sites B and C, the topsoil generally consists of non-liquefiable boulder stone or dredged silty clay.

Table 3.3. Simulation results of the liquefaction potential upon the Odaesan Earthquake-scale (M 4.8) and the Great East Japan Earthquake-scale (M 9.0) for the target areas

Site	No.	Soil Layer(m)	Liquefiable Layer(m)	Odaesan Earthquake-scale (M 4.8)					Great East Japan Earthquake-scale (M 9.0)				
				FS _{liquefaction}			LPI	Severity	FS _{liquefaction}			LPI	Severity
				F	AS	WS			F	AS	WS		
A	1	6.0	2.9	-	1.7	-	0.0	Very low	-	0.6	-	15.9	Very high
	2	5.8	0.9	-	0.9	-	3.5	Low	-	0.3	-	27.9	Very high
	3	7.0	2.2	-	1.0	-	1.2	Low	-	0.3	-	30.3	Very high
	4	16.0	15.9	1.9	2.6	-	0.0	Very low	0.6	1.0	-	20.1	Very high
	5	8.8	3.8	-	1.0	-	0.8	Low	-	0.4	-	30.3	Very high
	6	7.0	1.6	-	2.8	-	0.0	Very low	-	0.8	-	8.7	High
	7	18.6	18.5	0.8	1.8	-	9.1	High	0.3	0.5	-	40.3	Very high
	8	9.0	6.0	-	1.8	-	0.0	Very low	-	0.8	-	11.6	Very high
	9	11.5	8.8	-	1.9	-	0.0	Very low	-	0.8	-	7.9	High
	10	12.9	12.2	-	1.2	-	0.0	Very low	-	0.5	-	21.7	Very high
	11	29.5	29.0	0.8	5.4	-	9.7	High	0.4	2.7	-	30.6	Very high
	12	19.0	17.5	-	1.9	-	0.0	Very low	-	0.8	-	1.9	Low
B	13	26.4	19.6	2.3	4.0	7.9	0.0	Very low	1.2	2.0	2.5	0.0	Very Low
	14	26.7	20.4	2.9	5.0	7.5	0.0	Very low	1.4	2.4	3.0	0.0	Very Low
	15	24.2	17.5	2.3	4.9	-	0.0	Very low	1.1	2.1	-	0.0	Very Low
	16	36.0	29.0	2.2	7.1	-	0.0	Very low	1.2	3.7	-	0.0	Very Low
	17	16.5	9.5	2.2	2.8	-	0.0	Very low	1.1	1.3	-	0.0	Very Low
C	18	20.5	17.4	3.1	3.4	10.4	0.0	Very low	1.1	1.2	3.6	0.0	Very Low
	19	17.8	12.9	3.5	3.1	9.3	0.0	Very low	1.1	1.0	3.3	0.0	Very Low
	20	17.0	12.2	5.7	3.4	9.0	0.0	Very low	1.9	1.1	3.1	0.0	Very Low
	21	14.0	13.9	2.8	2.7	7.1	0.0	Very low	0.9	0.9	2.2	9.2	High
	22	13.1	8.1	3.6	4.6	10.0	0.0	Very low	1.2	1.5	3.3	0.0	Very Low

The assessment results were visualized on a location map to confirm the applicability of the proposed framework for real-time assessments of the liquefaction potential. Liquefaction hazard mappings of the target areas at the Incheon port are possible for the peak acceleration and FS values for each liquefiable soil layer and the LPI value and severity class of the type of liquefaction failure can be determined based on the GIS platform as shown in Fig. 3.2.

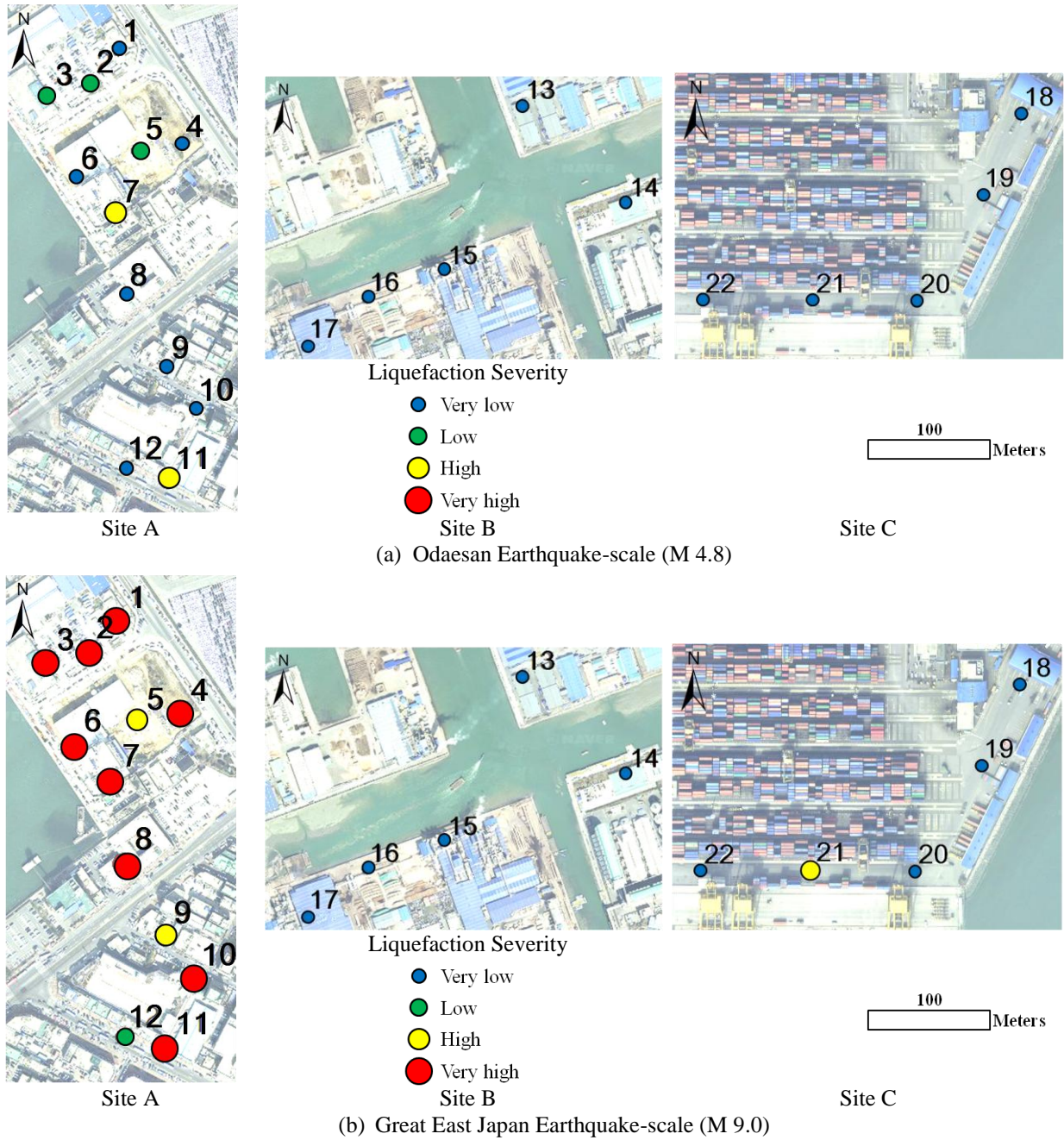


Figure 3.2. Liquefaction potential maps inferred from the severity class for an earthquake scenario with outcrop acceleration: (a) Odaesan Earthquake-scale (M 4.8) and (b) Great East Japan Earthquake-scale (M 9.0)

The liquefaction simulation was performed based on a systematic assessment of the liquefaction potential on a real-time basis, when earthquake occurred at harbor site. Accordingly, the developed system can be effectively utilized for disaster prevention measures to be taken against earthquakes.

4. Conclusions

In this study, a real-time assessment of the liquefaction potential was applied using the Incheon port as the target area based on a simplified systematic framework with a computer-based spatial information system. The LPI was computed by integrating the FS (CRR/CRS) values over the depths of liquefaction-susceptible soil layers, providing an estimate of liquefaction-related surface damage. For the application examples, two earthquake events were utilized to verify the real-time system. The simulation results were visualized on a liquefaction hazard map in an effort to confirm the

applicability of the proposed framework for the real-time assessment of the liquefaction potential.

ACKNOWLEDGEMENT

This study was supported mainly from the project ‘Establishment of seismic response monitoring system for port facilities and development of related technologies’ sponsored by the Ministry of Land, Transport and Maritime Affairs of Korea.

REFERENCES

- Baise, L. G., Higgins, R. B., and Brankman, C. M. (2006). Liquefaction hazard mapping—statistical and spatial characterization of susceptible units. *Journal of Geotechnical and Geoenvironmental Engineering*, **132**:6,705–715.
- C. Hsein Juang, Caroline J. Chen, Tao Jiang, and Ronald D. Andrus (2000), Risk-based liquefaction potential evaluation using standard penetration tests, *Canadian Geotechnical Journal*, **37**,1195-1208.
- Chung, J.W. and J. David Rogers (2011). Simplified Method for Spatial Evaluation of Liquefaction Potential in the St. Louis Area. *Journal of Geotechnical and Geoenvironmental Engineering*, **137**:5,505-515.
- Hayati, H., and Andrus, R. D. (2008). Liquefaction potential map of Charleston, South Carolina based in the 1886 Earthquake. *J. Geotech. Geoenviron. Eng.* **134**:6,815–828.
- Holzer, T.L., Bennett, M.J., Noce, T.E., Padovani, A.C., and Tinsley, J.C. (2006). Liquefaction hazard mapping with LPI in the Greater Oakland, California, area. *Earthquake Spectra*, **22**:3, 693-708.
- Ishihara, K. (1977). Simple Method of Analysis for Liquefaction of Sand Deposits During Earthquakes, *Soil and Foundations, JSSMFE*, **17**:3,1-8.
- Iwasaki, T., Tatsuoka, F., Tokida, K. and Yasuda, S. (1978). A Practical Method for Assessing Soil Liquefaction Potential Based on Case Studies at Various site in Japan. *5th Japan Earthquake Engineering Symposium*, **Vol II**: 641-648.
- Iwasaki, T., Tokida, K., Tatsuoka, F., Watanabe, S., Yasuda, S., and Sato, H. (1982). Microzonation for soil liquefaction potential using simplified methods. *Proceedings 3rd International Conference on Microzonation, Seattle, USA*. 1319-1330.
- Kim, H.S., Yoo, S.H, Jang, I.S and Chung, C.K. (2011), Real-time Seismic Damage Estimation for Harbor Site considering Dynamic Amplification Characteristics, *Proceedings Korean Marine Technology Society Joint National Conference*, **8**,1-4.
- Luna, R. (1995). Liquefaction evaluation using a spatial analysis system [Ph.D. thesis]: Atlanta, Georgia Institute of Technology.
- Luna, R. and Frost, J.D. (1998). Spatial liquefaction analysis system. *Journal of Computing in Civil Engineering*, **12**:1,48-56.
- Papathanassiou G (2008). LPI-based approach for calibrating the severity of liquefaction-induced failures and for assessing the probability of liquefaction surface evidence. *Engineering Geology*, **9**,694–104.
- Ronaldo Luna and J. David Frost (1998). Spatial Liquefaction Analysis System, *Journal of Computing in Civil Engineering*, **12**:1,350-356.
- Seed, H. B. and Idriss, I. M. (1971). Simplified Procedure for Evaluating Soil Liquefaction Potential. *Journal of Soil Mechanics and Foundation Division, ASCE*, **97**:SM9,221-235.
- Seed, H.B., Tokimatsu L.F., Harder, L.F. and Chung, R.M (1985). Influence of SPT procedures in soil liquefaction resistance evaluations. *Journal of Geotechnical Engineering*, **111**:12,1425-1445.
- Sonmez H (2003). Modification to the liquefaction potential index and liquefaction susceptibility mapping for a liquefaction-prone area (Inegol-Turkey). *Environmental Geology*, **44**:7,862–871.
- Toprak, S. and Holzer, T.L. (2003). Liquefaction potential index: field assessment. *Journal of Geotechnical and Geoenvironmental Engineering, ASCE*, **129**,315-322.
- Youd, T.L. and Perkins, D.M. (1978). Mapping liquefaction-induced ground failure potential. *Journal of the Geotechnical Engineering*, **104**,433-446.
- Youd, T.L. and Perkins, D.M. (1987). Mapping of liquefaction severity index. *Journal of Geotechnical Engineering*, **113**:11,1374-1392.